

Appearance of the universal value e^2/h of the zero-bias conductance in a Weyl semimetal-superconductor junction

Song-Bo Zhang,¹ Fabrizio Dolcini,² Daniel Breunig,¹ and Björn Trauzettel¹

¹*Institute for Theoretical Physics and Astrophysics,
University of Würzburg, D-97074 Würzburg, Germany*

²*Dipartimento di Scienza Applicata e Tecnologia del Politecnico di Torino, I-10129 Torino, Italy*
(Dated: July 23, 2018)

We study the differential conductance of a time-reversal symmetric Weyl semimetal-superconductor (N-S) junction with an s-wave superconducting state. We find that there exists an extended regime where the zero-bias differential conductance acquires the universal value e^2/h per unit channel, independent of the pairing and chemical potentials on each side of the junction, due to a perfect cancellation of Andreev and normal reflection contributions. This universal conductance can be attributed to the interplay of the unique spin/orbital-momentum locking and s-wave pairing that couples Weyl nodes of the same chirality. We expect that the universal conductance can serve as a robust and distinct signature for time-reversal symmetric Weyl fermions, and be observed in the recently discovered time-reversal symmetric Weyl semimetals.

PACS numbers:

Introduction.—A Weyl semimetal (WSM) is a three-dimensional (3D) topological phase of matter in which the conduction and valence bands touch linearly at discrete points, called Weyl nodes, in the Brillouin zone near the Fermi energy [1–5]. According to the fermion doubling, such Weyl nodes appear in pairs with opposite chirality [6, 7], linked to monopoles and anti-monopoles of the field of Berry curvature in momentum space. To ensure nonzero Berry curvature, a WSM must violate either inversion or time-reversal symmetry. This nontrivial momentum-space topology of WSMs gives rise to a variety of intriguing physical phenomena, such as surface Fermi arcs [1, 2], the chiral anomaly [8–10], and associated anomalous transport properties [11–27]. The actual discoveries of WSMs in a growing number of materials [28–43] have spurred the interest in investigating the interplay of such topological phase with other electronic phases and orders.

Recently, possibilities of superconducting states, doping- or proximity-induced, in WSMs have been discussed [44–59]. Most of the theoretical works investigating hybrid structures based on WSMs focus on the time-reversal broken case [60–66]. However, so far almost all the experimentally demonstrated WSMs break inversion symmetry but preserve time-reversal symmetry [31–36]. Importantly, while in a time-reversal broken Weyl superconductor the s-wave pairing couples electrons of opposite chirality, in the time-reversal symmetric case it couples electrons of the same chirality [44], so that distinct transport properties in N-S junctions could be expected.

In this work, we study a 3D time-reversal symmetric N-S junction constructed by a WSM and an s-wave superconducting Weyl metal. Near the Weyl nodes, the intra-orbital pairing dominates the superconducting state. Denoting by μ_N and μ_S the chemical potentials of the WSM

and superconductor, respectively, and by Δ_s the superconducting pairing potential, we find that in the regime $|\mu_N| \ll [|\Delta_s|^2 + \mu_S^2]^{1/2}$, the contributions of Andreev and normal reflections perfectly cancel at vanishing excitation energy. In this regime, the zero-bias differential conductance, thus, takes the universal value e^2/h per unit channel, independent of μ_N , μ_S , and Δ_s . We attribute this universal conductance to the interplay of the unique spin/orbital-momentum locking and s-wave pairing in the Weyl junction. We also discuss its robustness and expect that it can serve as a distinct signature for time-reversal symmetric Weyl fermions. We are confident that the universal conductance can be observed in the recently discovered time-reversal symmetric WSMs [39, 40].

Model Hamiltonian.—We start with a low-energy model for a time-reversal symmetric WSM [67]

$$\mathcal{H}_w = \sum_{\mathbf{k}} \psi_{\mathbf{k}}^\dagger H(\mathbf{k}) \psi_{\mathbf{k}}, \quad (1)$$

$$H(\mathbf{k}) = k_x s_x \sigma_z + k_y s_y \sigma_0 + (\kappa_0^2 - |\mathbf{k}|^2) g s_z \sigma_0 + \beta s_y \sigma_y - \alpha k_y s_x \sigma_y, \quad (2)$$

where $\mathbf{k} = (k_x, k_y, k_z)$ is the wave vector, the four-component spinor $\psi_{\mathbf{k}} = (c_{A,\uparrow,\mathbf{k}}, c_{A,\downarrow,\mathbf{k}}, c_{B,\uparrow,\mathbf{k}}, c_{B,\downarrow,\mathbf{k}})^T$ is written in terms of annihilation operators $c_{s,\sigma,\mathbf{k}}$ with spin indices $\sigma = \uparrow, \downarrow$ and orbital indices $s = A, B$. Here, σ_i ($i = 0, x, y, z$) are the 2×2 identity and Pauli matrices for the spin-1/2 space, and s_i ($i = 0, x, y, z$) for the orbital space. κ_0, α and β are real model parameters. The model (1) breaks inversion symmetry, i.e., $s_z H(\mathbf{k}) s_z \neq H(-\mathbf{k})$ by the β term, but preserves time-reversal symmetry as shown by $\sigma_y H^*(\mathbf{k}) \sigma_y = H(-\mathbf{k})$. Suppose $0 < \beta < \kappa_0$, the model (1) has four Weyl nodes at $\pm \mathbf{Q}_\pm$ where $\mathbf{Q}_\pm = (\beta, 0, \pm k_0)$ and $k_0 = [\kappa_0^2 - \beta^2]^{1/2}$.

Near the Weyl nodes, we can linearize the model (1) and rewrite it as a sum of four effective Hamiltonians,

each describes the electrons near one of the Weyl nodes

$$\mathcal{H}_w = \sum_{\gamma=1,2,3,4} \sum_{\mathbf{k}} \Psi_{\gamma,\mathbf{k}}^\dagger H_\gamma(\mathbf{k}) \Psi_{\gamma,\mathbf{k}}, \quad (3)$$

$$\begin{aligned} H_{1(2)}(\mathbf{k}) &= (k_x \mp \beta) \sigma_x + k_y \sigma_y + (k_z \mp k_0) \sigma_z, \\ H_{3(4)}(\mathbf{k}) &= (k_x \mp \beta) \sigma_x + k_y \sigma_y - (k_z \pm k_0) \sigma_z, \end{aligned} \quad (4)$$

where k_z has been re-scaled by $1/(2k_0)$ and k_y by $1/\alpha$, the indices $\gamma = 1, 2, 3, 4$ label the Weyl nodes at $\mathbf{Q}_+, -\mathbf{Q}_+, \mathbf{Q}_-, -\mathbf{Q}_-$, respectively, and $\sum_{\mathbf{k}}$ indicates that \mathbf{k} is confined to the vicinity of the Weyl nodes. The spinors $\Psi_{\gamma,\mathbf{k}} \equiv (\psi_{\gamma,\uparrow,\mathbf{k}}, \psi_{\gamma,\downarrow,\mathbf{k}})^T$ of Weyl nodes are given by $\Psi_{1,\mathbf{k}} = \Psi_{3,\mathbf{k}} = [c_{\uparrow,\mathbf{k}}^{(B)}, c_{\downarrow,\mathbf{k}}^{(A)}]^T$ and $\Psi_{2,\mathbf{k}} = \Psi_{4,\mathbf{k}} = [c_{\uparrow,\mathbf{k}}^{(A)}, c_{\downarrow,\mathbf{k}}^{(B)}]^T$ with $c_{\uparrow(\downarrow),\mathbf{k}}^{(s)} = (c_{s,\uparrow,\mathbf{k}} \pm c_{s,\downarrow,\mathbf{k}})/\sqrt{2}$. $H_1(\mathbf{k})$ and $H_2(\mathbf{k})$ describe the two Weyl nodes of positive chirality while $H_3(\mathbf{k})$ and $H_4(\mathbf{k})$ describe the two Weyl nodes of negative chirality. All the Weyl nodes consist of different orbitals and spins, and exhibit a nontrivial spin/orbital-momentum locking. They form two time-reversed pairs, i.e., $\sigma_y H_1^*(\mathbf{k}) \sigma_y = H_2(-\mathbf{k})$ and $\sigma_y H_3^*(\mathbf{k}) \sigma_y = H_4(-\mathbf{k})$, each of them with definite chirality.

Next, introducing the s-wave superconducting coupling with both intra- and inter-orbital pairing potentials and projecting onto the spinors of Weyl nodes, one can see that the inter-orbital pairing is strongly suppressed due to the mismatch of spins or momenta [68]. Suppose the Weyl nodes are well separated and the chemical potential is close to the Weyl nodes, then only the intra-orbital pairing is important and reads

$$\mathcal{H}_S = \mathcal{H}_S^+ + \mathcal{H}_S^-, \quad (5)$$

$$\mathcal{H}_S^+ = \sum_{\mathbf{k}} ' \left[\left(\Delta_s c_{1,\uparrow,\mathbf{k}}^\dagger c_{2,\downarrow,-\mathbf{k}}^\dagger + h.c. \right) + (1 \leftrightarrow 2) \right],$$

$$\mathcal{H}_S^- = \sum_{\mathbf{k}} ' \left[\left(\Delta_s c_{3,\uparrow,\mathbf{k}}^\dagger c_{4,\downarrow,-\mathbf{k}}^\dagger + h.c. \right) + (3 \leftrightarrow 4) \right].$$

The pairing potential Δ_s couples electrons on Weyl nodes stemming from the time-reversed pairs. The whole system can thus be understood as two effectively independent and equivalent subsystems with opposite chirality. In the following, we will discuss the physics of the subsystem with positive chirality.

Using the Nambu spinor in real space for positive chirality $\tilde{\Psi}(\mathbf{r}) = [c_{1,\uparrow}(\mathbf{r}), c_{1,\downarrow}(\mathbf{r}), c_{2,\uparrow}(\mathbf{r}), c_{2,\downarrow}(\mathbf{r}), c_{1,\downarrow}^\dagger(\mathbf{r}), -c_{1,\uparrow}^\dagger(\mathbf{r}), c_{2,\downarrow}^\dagger(\mathbf{r}), -c_{2,\uparrow}^\dagger(\mathbf{r})]^T$, we recast the Hamiltonian in a Bogoliubov-de Gennes (BdG) form

$$\mathcal{H}_+ = \frac{1}{2} \int d\mathbf{r} \Phi^\dagger(\mathbf{r}) H_{\text{BdG}} \Phi(\mathbf{r}), \quad (6)$$

$$H_{\text{BdG}} = (-i\partial_{\mathbf{r}} \cdot \boldsymbol{\sigma} - \mu\sigma_0) \tau_0 \nu_z + |\Delta_s| e^{i\phi\nu_z} \sigma_0 \tau_x \nu_x, \quad (7)$$

where $\Delta_s(\mathbf{r}) = |\Delta_s(\mathbf{r})| e^{i\phi(\mathbf{r})}$. We have introduced the identity and Pauli matrices ν_i and τ_i ($i = 0, x, y, z$) for electron-hole and Weyl-node degrees of freedom, respectively, and moved the k_0 and β dependence into the

wave function by performing a unitary transformation $\Phi(\mathbf{r}) = e^{i(k_0 z \sigma_z + \beta x \sigma_x) \tau_z \nu_z} \tilde{\Psi}(\mathbf{r})$. In a uniform system, the eigenenergies are given by $\varepsilon = \pm[|\Delta_s|^2 + (|\mathbf{k}| \pm \mu)^2]^{1/2}$. The superconductor is fully gapped. The BdG Hamiltonian (7) decouples into two 4×4 identical blocks which can be treated separately. We will consider one block which is enough to fully describe the junction problem.

Reflection probabilities in a Weyl N-S junction.—The time-reversal symmetric Weyl N-S junction can be described by the BdG Hamiltonian (7) with $\Delta_s(z) = \Delta e^{i\phi} \Theta(z)$ and $\mu(z) = \mu_N \Theta(-z) + \mu_S \Theta(z)$. Here $\Theta(z)$ is the Heaviside step function, $\Delta > 0$ and a constant superconducting phase ϕ are assumed. The wave vector $\mathbf{k}_{\parallel} = (k_x, k_y)$ parallel to the N-S interface is conserved. We can treat each \mathbf{k}_{\parallel} separately and work with a quasi-1D junction problem.

Assuming first a clean interface and matching the wave function at the interface, the probabilities of Andreev and normal reflections at an excitation energy $\varepsilon \geq 0$, in general, can be expressed as

$$R_{eh}(\varepsilon, \mathbf{k}_{\parallel}) = |\cos(2\alpha_e) \cos(2\alpha_h)| |\sin(\tilde{\alpha}_e - \tilde{\alpha}_h)/\mathcal{Z}|^2, \quad (8)$$

$$R_{ee}(\varepsilon, \mathbf{k}_{\parallel}) = |\mathcal{Y}/\mathcal{Z}|^2, \quad (9)$$

respectively, where $\mathcal{Z} = e^{i\beta} \cos(\alpha_e + \tilde{\alpha}_e) \sin(\alpha_h + \tilde{\alpha}_h) - e^{-i\beta} \cos(\alpha_e + \tilde{\alpha}_h) \sin(\alpha_h + \tilde{\alpha}_e)$, $\mathcal{Y} = e^{i\beta} \sin(\alpha_e - \tilde{\alpha}_e) \sin(\alpha_h + \tilde{\alpha}_h) - e^{-i\beta} \sin(\alpha_e - \tilde{\alpha}_h) \sin(\alpha_h + \tilde{\alpha}_e)$, $\alpha_{e(h)} = \arctan(k_{\parallel}/k_{e(h)})/2$, $\tilde{\alpha}_{e(h)} = \arctan(k_{\parallel}/k_{eq(hq)})/2$ and $k_{\parallel} = |\mathbf{k}_{\parallel}|$. The perpendicular momenta for the electron (hole) and electronlike (holelike) quasiparticle are $k_{e(h)} = \text{sgn}(\varepsilon \pm \mu_N + k_{\parallel}) [(\varepsilon \pm \mu_N)^2 - k_{\parallel}^2]^{1/2}$ and $k_{eq(hq)} = \text{sgn}\{\varepsilon \pm \text{sgn}(\mu_S \pm k_{\parallel}) [\Delta^2 + (\mu_S \pm k_{\parallel})^2]^{1/2}\} [(\mu_S \pm \Omega)^2 - k_{\parallel}^2]^{1/2}$, respectively. For subgap energies $\varepsilon \leq \Delta$, $\Omega = i[\Delta^2 - \varepsilon^2]^{1/2}$ and $\beta = \arccos(\varepsilon/\Delta)$, while for supragap energies $\varepsilon > \Delta$, $\Omega = \text{sgn}(\varepsilon)[\varepsilon^2 - \Delta^2]^{1/2}$ and $\beta = -i \text{arccosh}(\varepsilon/\Delta)$. Note that $\alpha_{e(h)}$ is always real while $\tilde{\alpha}_{e(h)}$ can be complex. Detailed derivation is provided in [68]. For subgap energies, $\varepsilon \leq \Delta$, $R_{eh} + R_{ee} = 1$, whereas for supragap energies, $\varepsilon > \Delta$, $R_{eh} + R_{ee} < 1$. For a generic oblique incidence ($\mathbf{k}_{\parallel} \neq 0$) both normal and Andreev reflection are present, and only for normal incidence ($\mathbf{k}_{\parallel} = 0$) one has perfect Andreev reflection below the gap, since Eqs. (8) and (9) reduce to $R_{eh} = |e^{-2i\beta}|$ and $R_{ee} = 0$.

Differential conductance.—At zero temperature, the differential conductance (per unit area) in the N-S junction is given by [69]

$$\frac{dI}{dV} \equiv \frac{e^2}{h} \int \frac{d^2 \mathbf{k}_{\parallel}}{(2\pi)^2} [1 - R_{ee}(eV, \mathbf{k}_{\parallel}) + R_{eh}(eV, \mathbf{k}_{\parallel})], \quad (10)$$

where eV is the bias voltage. Note that only real k_e contribute in Eq. (10). We normalize the conductance to the value $G_0 = e^2(\mu_N + eV)^2/(4\pi\hbar)$, corresponding to the number of available channels at energy $\mu_N + eV$ on the N side. With the expressions (8) and (9) in Eq. (10), we are able to analyze the behaviors of the conductance. We

concentrate, in the following, on two particular parameter regimes: (i) $\mu_S = \mu_N$ (Δ arbitrary); and (ii) $\mu_S \gg \Delta$ (μ_N arbitrary) [77], which have a distinct zero-bias feature in common (see below).

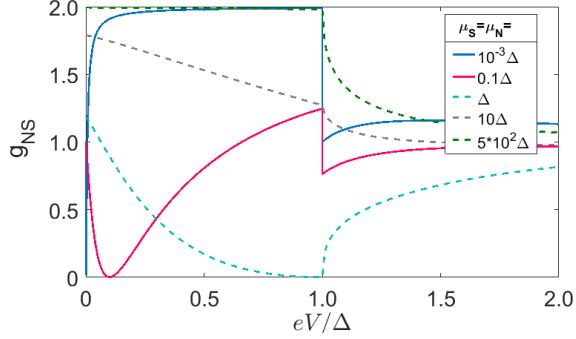


Figure 1: Normalized conductance g_{NS} as a function of bias for various values of $\mu_N = \mu_S$.

For regime (i), $\mu_S = \mu_N$, the normalized conductance $g_{NS} \equiv G_0^{-1} dI/dV$ [78] as a function of eV is plotted in Fig. 1. At large bias $eV \gg \Delta$, all curves converge to unity. This is expected since at large excitation energies the influence of superconductivity is negligible, which together with an identical chemical potential on both sides makes the interface transparent. The g_{NS} - eV relation is rich in the subgap region, depending on the ratio μ_N/Δ . For $\mu_N/\Delta \gg 1$, the Fermi momentum mismatch of the two sides is negligible, i.e., $k_{eq(hq)} \approx k_{e(h)}$, thus normal reflection is suppressed, leading to perfect Andreev reflection with $g_{NS} = 2$. Similar behavior occurs for conventional electron systems [69]. For smaller μ_N , but $\mu_N > \Delta$, g_{NS} bends down and even shows a dip at $eV = \Delta$. For $0 < \mu_N < \Delta$, g_{NS} vanishes at $eV = \mu_N$ as no hole state is available for Andreev reflection. This is typical for gapless Dirac systems [70]. In the limit $\mu_N/\Delta \ll 1$, specular Andreev reflection dominates in the bias region $\mu_N < eV < \Delta$ and gives rise to $g_{NS} = 2$ [68]. Nevertheless, in the limit of low biases, g_{NS} approaches unity for $\mu_N/\Delta \ll 1$ (see solid curves in Fig. 1), implying the universal conductance e^2/h per unit channel.

Let us now consider regime (ii), $\mu_S \gg \Delta$, which corresponds to the most relevant experimental condition and is depicted in Fig. 2. For $\mu_N > \mu_S$, g_{NS} varies little in the subgap region and it decreases smoothly to a constant at large bias. With decreasing μ_N , g_{NS} increases in the subgap region or at large bias. For $\mu_N = \mu_S$, g_{NS} is maximized for any bias and shows perfect Andreev reflection with $g_{NS} = 2$ in the subgap region. For $\mu_N < \Delta$, the vanishing of g_{NS} can also be observed at $eV = \mu_N$ where no Andreev reflection is allowed. Most remarkably, for $\mu_N \ll \mu_S$, one can notice again that all the curves approach unity in the limit of low biases, despite that they vary substantially away from zero bias, and converge to a constant $4 \log(2) - 2$ at large bias (see solid curves and inset in Fig. 2).

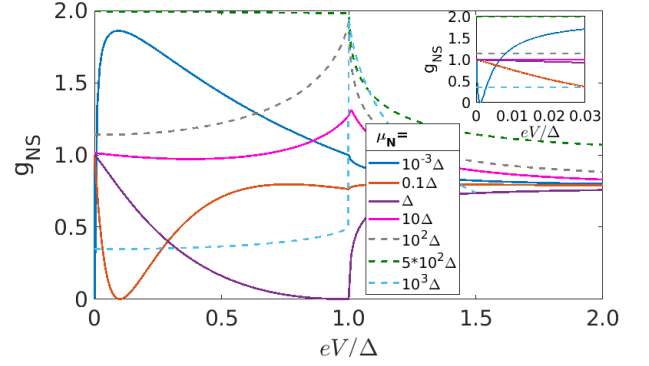


Figure 2: Normalized conductance g_{NS} as a function of bias for fixed $\mu_S = 5 \times 10^2 \Delta$ and various values of μ_N . Inset is the zoom-in in the limit of low biases.

Zero-bias conductance and universal value.—Figure 3 focuses on the behavior of the zero-bias conductance g_{NS} . In particular, Fig. 3(a) displays various salient features of g_{NS} as a function of μ_S and μ_N . First, g_{NS} is centrosymmetric in the phase space $\{\mu_N, \mu_S\}$, as a hallmark of particle-hole symmetry of the system. Second, g_{NS} shows a ridge along the line $\mu_N = \mu_S$ where the small Fermi momentum mismatch strongly suppresses normal reflection. In contrast, when $|\mu_S| \ll |\mu_N|$, the Fermi momentum mismatch is large and normal reflection is enhanced, we have thus vanishing g_{NS} . Finally, g_{NS} is always smaller than unity in the bipolar regime with $\mu_N \mu_S < 0$, implying that the normal reflection contribution is larger than the Andreev reflection contribution.

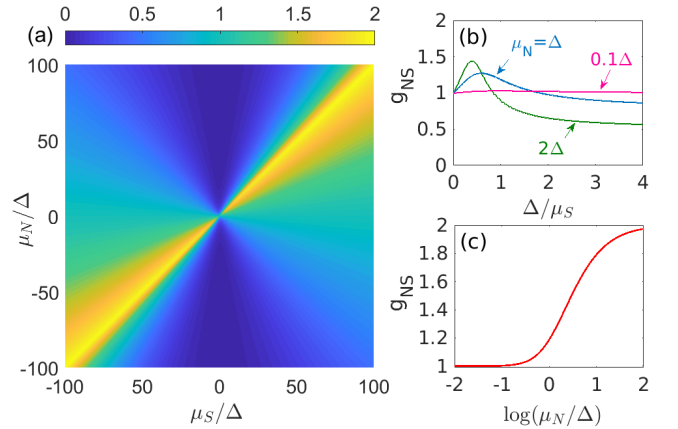


Figure 3: (a) The zero-bias conductance g_{NS} as a function of μ_S and μ_N . (b) g_{NS} as a function of Δ/μ_S for various values of μ_N . (c) semi-logarithmic plot of g_{NS} as a function of $\mu_S = \mu_N$.

Figure 3(b) shows the behavior of g_{NS} as a function of Δ/μ_S for various values of μ_N . Figure 3(c) instead displays g_{NS} with respect to $\mu_N = \mu_S$. The universal conductance e^2/h clearly appears in the regime:

$$|\mu_N| \ll \sqrt{\Delta^2 + \mu_S^2}, \quad (11)$$

where the Fermi momenta on the two sides of the interface are very different, i.e., $|k_e| \ll |k_{eq}|$. We note that such regime corresponds to an ideal semimetal phase on the N side, which should be experimentally accessible. To understand the occurrence of the universal conductance, we focus on the regime (11) and analyze our analytical results. Since only real k_e contribute to the conductance given by Eq. (10), the channels with $k_{\parallel} < |\mu_N|$ are relevant. From the BdG Hamiltonian (7), we observe that while on the N side the parallel wave vector \mathbf{k}_{\parallel} , which couples different spins and orbitals, is significant, on the S side it becomes negligible compared to the perpendicular momentum, i.e., $k_{\parallel} \ll |k_{eq}| \approx [\Delta^2 + \mu_S^2]^{1/2}$. Thus, the A- and B-orbital components are decoupled from each other on the S side. As a result, the reflection probabilities at zero energy reduce to

$$R_{eh}(0, \mathbf{k}_{\parallel}) = 1 - |k_{\parallel}/\mu_N|^2, \quad (12)$$

$$R_{ee}(0, \mathbf{k}_{\parallel}) = |k_{\parallel}/\mu_N|^2. \quad (13)$$

They become functions of a single parameter $|k_{\parallel}/\mu_N|$. Notably, normal and Andreev reflections have opposite contribution to the conductance, according to Eq. (10). Plugging Eqs. (12) and (13) into Eq. (10), it is straightforward to see that the contributions from Andreev and normal reflections cancel each other perfectly, giving rise to the universal conductance e^2/h per unit channel. The perfect cancellation in the 3D Weyl junction can be understood as a result of the unique spin/orbital-momentum locking and s-wave pairing, which can be inferred from the analog of the Weyl system to a 1D ferromagnet-superconductor junction [68].

Robustness of the universal value.—We note that in a conventional electron system with parabolic spectrum, the zero-bias conductance can also exhibit a universal value in the regime (11). However, it is trivially zero. Indeed, since in that case velocity and current are linear in momentum, for large momentum mismatch, the conservation of the flux at the interface is only possible if the flux vanishes. By contrast, in a Dirac system, the Fermi velocity is constant and the flux conservation is less sensitive to the Fermi momentum mismatch. As a consequence, non-vanishing flux and conductance are possible. In graphene, a 2D Dirac system, a finite characteristic value ($4e^2/3h$) of the zero-bias conductance can be found [70]. However, the instabilities of the 2D Dirac cone to small perturbations, such the intrinsic spin-orbit coupling [71] or the coupling to the substrate [72], likely mask such effect. In fact, to the authors' knowledge, the value $4e^2/3h$ in graphene has never been observed experimentally. By contrast, the Weyl nodes in a WSM are topologically protected and cannot be gapped out. Therefore, we expect that the universal conductance e^2/h found here is accessible in experiments.

Finally, we stress that the universal conductance predicted by us is robust in the presence of an interface bar-

rier, due to Klein tunneling [68, 73]. The interface barrier can be modeled by a potential term $V_0 \nu_z \Theta(z+d) \Theta(-z)$ in the BdG Hamiltonian, where we assume the barrier length $d \rightarrow 0$ and potential $V_0 \rightarrow \infty$ but the barrier strength $\chi \equiv V_0 d$ remains finite [74]. Then, g_{NS} is an oscillation function of χ with a period π . In the regime (11), g_{NS} oscillates slightly around the universal value, as shown in Fig. 3. Note that if the system is not deep in the regime (11), only a small deviation from e^2/h appears. Therefore, the universal conductance can be used as a distinct signature for time-reversal symmetric Weyl fermions.

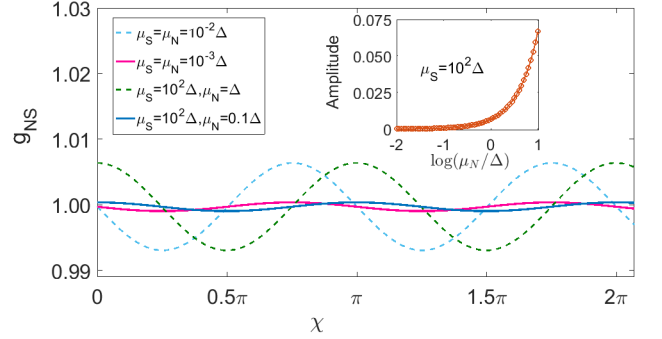


Figure 4: The zero-bias conductance g_{NS} as a function of the barrier strength χ for various μ_S and μ_N . Inset is the semi-logarithmic plot of the oscillation amplitudes as a function of μ_N for fixed $\mu_S = 10^2 \Delta$.

Experimental relevance.—Recently, an ideal time-reversal symmetric WSM phase has been proposed in 3D HgTe under compressive strain [39, 40]. There are likely four pairs of Weyl nodes in the WSM phase [40]. However, as long as the Fermi energy is close enough to the Weyl nodes, the system can be decoupled to multiple equivalent time-reversed subsystems. Then our analysis and main results should hold. Importantly, superconductivity in 3D compressively strained HgTe could be realized by proximity to a conventional s-wave superconductor, similar to the case of tensilely strained HgTe, a 3D topological insulator [75, 76]. Therefore, we expect that the universal conductance e^2/h could be measured on compressively strained HgTe systems.

Summary.—We have analyzed a time-reversal symmetric Weyl N-S junction with an s-wave superconducting pairing state. In an accessible regime, the zero-bias differential conductance takes the universal value e^2/h per unit channel, independent of the pairing and chemical potentials, as the Andreev and normal reflection contributions perfectly cancel at vanishing excitation energy. The universal conductance can be understood as a consequence of the interplay of the unique spin/orbital-momentum locking and s-wave pairing in the WSM system.

Acknowledgments.—We thank Jian Li, Benedikt Scharf, Martin Stehno, and Xianxin Wu for valuable

discussions. This work was supported by the DFG (SPP1666 and SFB1170 "ToCoTronics") and the ENB Graduate School on "Topological Insulators".

-
- [1] X. Wan, A. M. Turner, A. Vishwanath, and S. Y. Savrasov, *Phys. Rev. B* **83**, 205101 (2011).
 - [2] A. A. Burkov and L. Balents, *Phys. Rev. Lett.* **107**, 127205 (2011).
 - [3] A. M. Turner and A. Vishwanath, ArXiv e-prints (2013), [arXiv:1301.0330 \[cond-mat.str-el\]](#).
 - [4] P. Hosur and X. Qi, *C. R. Phys.* **14**, 857 (2013).
 - [5] N. P. Armitage, E. J. Mele, and A. Vishwanath, ArXiv e-prints (2017), [arXiv:1705.01111 \[cond-mat.str-el\]](#).
 - [6] H. B. Nielsen and M. Ninomiya, *Phys. Lett. B* **105**, 219 (1981).
 - [7] H. B. Nielsen and M. Ninomiya, *Nucl. Phys. B* **185**, 20 (1981).
 - [8] H. B. Nielsen and M. Ninomiya, *Phys. Lett. B* **130**, 389 (1983).
 - [9] V. Aji, *Phys. Rev. B* **85**, 241101 (2012).
 - [10] P. Goswami and S. Tewari, *Phys. Rev. B* **88**, 245107 (2013).
 - [11] K. Fukushima, D. E. Kharzeev, and H. J. Warringa, *Phys. Rev. D* **78**, 074033 (2008).
 - [12] G. Xu, H. M. Weng, Z. J. Wang, X. Dai, and Z. Fang, *Phys. Rev. Lett.* **107**, 186806 (2011).
 - [13] K. Y. Yang, Y. M. Lu, and Y. Ran, *Phys. Rev. B* **84**, 075129 (2011).
 - [14] A. A. Zyuzin and A. A. Burkov, *Phys. Rev. B* **86**, 115133 (2012).
 - [15] P. Hosur, S. A. Parameswaran, and A. Vishwanath, *Phys. Rev. Lett.* **108**, 046602 (2012).
 - [16] D. T. Son and B. Z. Spivak, *Phys. Rev. B* **88**, 104412 (2013).
 - [17] A. A. Burkov, *Phys. Rev. Lett.* **113**, 187202 (2014).
 - [18] E. V. Gorbar, V. A. Miransky, and I. A. Shovkovy, *Phys. Rev. B* **89**, 085126 (2014).
 - [19] A. A. Burkov, *Phys. Rev. Lett.* **113**, 247203 (2014).
 - [20] A. C. Potter, I. Kimchi, and A. Vishwanath, *Nat. Commun.* **5**, 5161 (2014).
 - [21] H.-Z. Lu, S.-B. Zhang, and S.-Q. Shen, *Phys. Rev. B* **92**, 045203 (2015).
 - [22] S. A. Parameswaran, T. Grover, D. A. Abanin, D. A. Pesin, and A. Vishwanath, *Phys. Rev. X* **4**, 031035 (2014).
 - [23] J. Zhou, H. R. Chang, and D. Xiao, *Phys. Rev. B* **91**, 035114 (2015).
 - [24] S.-B. Zhang, H.-Z. Lu, and S.-Q. Shen, *New J. Phys.* **18**, 053039 (2016).
 - [25] C. Zhang, S. Y. Xu, I. Belopolski, Z. Yuan, Z. Lin, B. Tong, N. Alidoust, C. C. Lee, S. M. Huang, T. R. Chang, H. T. Jeng, H. Lin, M. Neupane, D. S. Sanchez, H. Zheng, G. Bian, J. Wang, C. Zhang, H. Z. Lu, S. Q. Shen, T. Neupert, M. Z. Hasan, and S. Jia, *Nat. Commun.* **7**, 10735 (2016).
 - [26] H. Li, H. T. He, H. Z. Lu, H. C. Zhang, H. C. Liu, R. Ma, Z. Y. Fan, S. Q. Shen, and J. N. Wang, *Nat. Commun.* **6**, 10301 (2016).
 - [27] Q. Li, D. E. Kharzeev, C. Zhang, Y. Huang, I. Pletikoscic, A. V. Fedorov, R. D. Zhong, J. A. Schneeloch, G. D. Gu, and T. Valla, *Nat. Phys.* **12**, 550 (2016).
 - [28] G. B. Halász and L. Balents, *Phys. Rev. B* **85**, 035103 (2012).
 - [29] M. Hirayama, R. Okugawa, S. Ishibashi, S. Murakami, and T. Miyake, *Phys. Rev. Lett.* **114**, 206401 (2015).
 - [30] J. Liu and D. Vanderbilt, *Phys. Rev. B* **90**, 155316 (2014).
 - [31] S. Y. Xu, I. Belopolski, N. Alidoust, M. Neupane, G. Bian, C. L. Zhang, R. Sankar, G. Q. Chang, Z. J. Yuan, C. C. Lee, S. M. Huang, H. Zheng, J. Ma, D. S. Sanchez, B. K. Wang, A. Bansil, F. C. Chou, P. P. Shibayev, H. Lin, S. Jia, and M. Z. Hasan, *Science* **349**, 613 (2015).
 - [32] L. X. Yang, Z. K. Liu, Y. Sun, H. Peng, H. F. Yang, T. Zhang, B. Zhou, Y. Zhang, Y. F. Guo, M. Rahn, D. Prabhakaran, Z. Hussain, S.-K. Mo, C. Felser, B. Yan, and Y. L. Chen, *Nat Phys* **11**, 728 (2015).
 - [33] B. Q. Lv, H. M. Weng, B. B. Fu, X. P. Wang, H. Miao, J. Ma, P. Richard, X. C. Huang, L. X. Zhao, G. F. Chen, Z. Fang, X. Dai, T. Qian, and H. Ding, *Phys. Rev. X* **5**, 031013 (2015).
 - [34] B. Q. Lv, N. Xu, H. M. Weng, J. Z. Ma, P. Richard, X. C. Huang, L. X. Zhao, G. F. Chen, C. E. Matt, F. Bisti, V. N. Strocov, J. Mesot, Z. Fang, X. Dai, T. Qian, M. Shi, and H. Ding, *Nat. Phys.* **11**, 724 (2015).
 - [35] S. Y. Xu, N. Alidoust, I. Belopolski, Z. Yuan, G. Bian, T. R. Chang, H. Zheng, V. N. Strocov, D. S. Sanchez, G. Chang, C. Zhang, D. Mou, Y. Wu, L. Huang, C. C. Lee, S. M. Huang, B. Wang, A. Bansil, H. T. Jeng, T. Neupert, A. Kaminski, H. Lin, S. Jia, and M. Zahid Hasan, *Nat. Phys.* **11**, 294 (2015).
 - [36] N. Xu, H. M. Weng, B. Q. Lv, C. E. Matt, J. Park, F. Bisti, V. N. Strocov, D. Gawryluk, E. Pomjakushina, K. Conder, N. C. Plumb, M. Radovic, G. Autes, O. V. Yazyev, Z. Fang, X. Dai, T. Qian, J. Mesot, H. Ding, and M. Shi, *Nat. Commun.* **7** (2016).
 - [37] S. M. Huang, S. Y. Xu, I. Belopolski, C. C. Lee, G. Chang, B. K. Wang, N. Alidoust, G. Bian, M. Neupane, C. Zhang, S. Jia, A. Bansil, H. Lin, and M. Z. Hasan, *Nat. Commun.* **6**, 7373 (2015).
 - [38] H. M. Weng, C. Fang, Z. Fang, B. A. Bernevig, and X. Dai, *Phys. Rev. X* **5**, 011029 (2015).
 - [39] T. Rauch, S. Achilles, J. Henk, and I. Mertig, *Phys. Rev. Lett.* **114**, 236805 (2015).
 - [40] J. Ruan, S.-K. Jian, H. Yao, H. Zhang, S.-C. Zhang, and D. Xing, *Nat. Commun.* **7**, 11136 (2016).
 - [41] J. Ruan, S.-K. Jian, D. Zhang, H. Yao, H. Zhang, S.-C. Zhang, and D. Xing, *Phys. Rev. Lett.* **116**, 226801 (2016).
 - [42] S. Jia, S.-Y. Xu, and M. Z. Hasan, *Nat Mater* **15**, 1140 (2016).
 - [43] S. Murakami, M. Hirayama, R. Okugawa, and T. Miyake, *Science Adv.* **3**, e1602680 (2017).
 - [44] T. Meng and L. Balents, *Phys. Rev. B* **86**, 054504 (2012).
 - [45] G. Y. Cho, J. H. Bardarson, Y.-M. Lu, and J. E. Moore, *Phys. Rev. B* **86**, 214514 (2012).
 - [46] V. Shivamoggi and M. J. Gilbert, *Phys. Rev. B* **88**, 134504 (2013).
 - [47] S. A. Yang, H. Pan, and F. Zhang, *Phys. Rev. Lett.* **113**, 046401 (2014).
 - [48] P. Hosur, X. Dai, Z. Fang, and X.-L. Qi, *Phys. Rev. B* **90**, 045130 (2014).
 - [49] U. Khanna, A. Kundu, S. Pradhan, and S. Rao, *Phys. Rev. B* **90**, 195430 (2014).
 - [50] H. Wei, S.-P. Chao, and V. Aji, *Phys. Rev. B* **89**, 014506 (2014).

- (2014).
- [51] M. H. Fischer, T. Neupert, C. Platt, A. P. Schnyder, W. Hanke, J. Goryo, R. Thomale, and M. Sigrist, *Phys. Rev. B* **89**, 020509 (2014).
 - [52] G. Bednik, A. A. Zyuzin, and A. A. Burkov, *Phys. Rev. B* **92**, 035153 (2015).
 - [53] B. Lu, K. Yada, M. Sato, and Y. Tanaka, *Phys. Rev. Lett.* **114**, 096804 (2015).
 - [54] Y. Li and F. D. M. Haldane, ArXiv e-prints (2015), [arXiv:1510.01730 \[cond-mat.str-el\]](#).
 - [55] S.-K. Jian, Y.-F. Jiang, and H. Yao, *Phys. Rev. Lett.* **114**, 237001 (2015).
 - [56] B. Liu, X. Li, L. Yin, and W. V. Liu, *Phys. Rev. Lett.* **114**, 045302 (2015).
 - [57] A. Chen and M. Franz, *Phys. Rev. B* **93**, 201105 (2016).
 - [58] R. Wang, L. Hao, B. Wang, and C. S. Ting, *Phys. Rev. B* **93**, 184511 (2016).
 - [59] M. D. Bachmann, N. Nair, F. Flicker, R. Ilan, T. Meng, N. J. Ghimire, E. D. Bauer, F. Ronning, J. G. Analytis, and P. J. W. Moll, *Science Adv.* **3**, e1602983 (2017).
 - [60] S. Uchida, T. Habe, and Y. Asano, *J. Phys. Soc. Jpn.* **83**, 064711 (2014).
 - [61] W. Chen, L. Jiang, R. Shen, L. Sheng, B. G. Wang, and D. Y. Xing, *Europhys. Lett.* **103**, 27006 (2013).
 - [62] Y. Kim, M. J. Park, and M. J. Gilbert, *Phys. Rev. B* **93**, 214511 (2016).
 - [63] U. Khanna, D. K. Mukherjee, A. Kundu, and S. Rao, *Phys. Rev. B* **93**, 121409 (2016).
 - [64] K. A. Madsen, E. J. Bergholtz, and P. W. Brouwer, *Phys. Rev. B* **95**, 064511 (2017).
 - [65] N. Bovenzi, M. Breitkreiz, P. Baireuther, T. E. O'Brien, J. Tworzydło, I. Adagideli, and C. W. J. Beenakker, *Phys. Rev. B* **96**, 035437 (2017).
 - [66] D. K. Mukherjee, S. Rao, and A. Kundu, *Phys. Rev. B* **96**, 161408 (2017).
 - [67] This model is based on the lattice model proposed by Kourtis, J. Li, Z. Wang, A. Yazdani, and B. A. Bernevig, *Phys. Rev. B* **93**, 041109 (2016).
 - [68] See Supplemental Material for detailed calculations and analysis.
 - [69] G. E. Blonder, M. Tinkham, and T. M. Klapwijk, *Phys. Rev. B* **25**, 4515 (1982).
 - [70] C. W. J. Beenakker, *Phys. Rev. Lett.* **97**, 067007 (2006).
 - [71] C. L. Kane and E. J. Mele, *Phys. Rev. Lett.* **95**, 226801 (2005).
 - [72] G. Giovannetti, P. A. Khomyakov, G. Brocks, P. J. Kelly, and J. van den Brink, *Phys. Rev. B* **76**, 073103 (2007).
 - [73] M. I. Katsnelson, K. S. Novoselov, and A. K. Geim, *Nat. Phys.* **2**, 620 (2006).
 - [74] S. Bhattacharjee and K. Sengupta, *Phys. Rev. Lett.* **97**, 217001 (2006).
 - [75] L. Maier, J. B. Oostinga, D. Knott, C. Brüne, P. Virtanen, G. Tkachov, E. M. Hankiewicz, C. Gould, H. Buhmann, and L. W. Molenkamp, *Phys. Rev. Lett.* **109**, 186806 (2012).
 - [76] J. Wiedenmann, E. Liebhaber, J. Kübert, E. Bocquillon, P. Burset, C. Ames, H. Buhmann, T. M. Klapwijk, and L. W. Molenkamp, *Phys. Rev. B* **96**, 165302 (2017).
 - [77] but μ_N and μ_S are still small enough so that the linearized model (4) is applicable
 - [78] here and everywhere afterwards we refer the normalized conductance to g_{NS}

Supplemental material

In this Supplemental Material, we show (S1) the derivation of the effective Hamiltonian for the s-wave superconducting pairing; (S2) Transport probabilities of the Weyl N-S junction; (S3) Analogy of the Weyl junction to a 1D ferromagnet-superconductor (F-S) junction; (S4) Effect of an interface barrier on the conductance.

S1. EFFECTIVE HAMILTONIAN FOR THE S-WAVE SUPERCONDUCTING COUPLING

The s-wave superconducting coupling with both intra- and inter-orbital pairing potentials is given by

$$\mathcal{H}_S = - \sum_{s=A,B} \sum_{\mathbf{k}} \left(\Delta_s c_{s,\uparrow,\mathbf{k}}^\dagger c_{s,\downarrow,-\mathbf{k}}^\dagger + h.c. \right) - \sum_{\mathbf{k}} [(\tilde{\Delta}_s c_{A,\uparrow,\mathbf{k}}^\dagger c_{B,\downarrow,-\mathbf{k}}^\dagger + h.c.) + (A \leftrightarrow B)], \quad (\text{S1.1})$$

where Δ_s and $\tilde{\Delta}_s$ measure the amplitudes of the intra- and inter-orbital pairing potentials. Under the unitary transformation $c_{\uparrow(\downarrow),\mathbf{k}}^{(s)} = (c_{s,\uparrow,\mathbf{k}} \pm c_{s,\downarrow,\mathbf{k}})/\sqrt{2}$, $s = A, B$, we have

$$\sum_{\mathbf{k}} (c_{s,\uparrow,\mathbf{k}} c_{s',\downarrow,-\mathbf{k}} + c_{s',\uparrow,\mathbf{k}} c_{s,\downarrow,-\mathbf{k}}) = \sum_{\mathbf{k}} \left[c_{\downarrow,\mathbf{k}}^{(s)} c_{\uparrow,-\mathbf{k}}^{(s')} + c_{\downarrow,\mathbf{k}}^{(s')} c_{\uparrow,-\mathbf{k}}^{(s)} \right]. \quad (\text{S1.2})$$

Thus, we can rewrite Eq. (S1.1) in the Nambu spinor

$$\Psi_{\mathbf{k}} = \left[c_{\uparrow,\mathbf{k}}^{(A)}, c_{\downarrow,\mathbf{k}}^{(A)}, c_{\uparrow,\mathbf{k}}^{(B)}, c_{\downarrow,\mathbf{k}}^{(B)}, c_{\downarrow,-\mathbf{k}}^{(A)\dagger}, -c_{\uparrow,-\mathbf{k}}^{(A)\dagger}, c_{\downarrow,-\mathbf{k}}^{(B)\dagger}, -c_{\uparrow,-\mathbf{k}}^{(B)\dagger} \right]^T, \quad (\text{S1.3})$$

as

$$\mathcal{H}_S = \frac{1}{2} \sum_{\mathbf{k}} \Psi_{\mathbf{k}}^\dagger H_\Delta \Psi_{\mathbf{k}}, \quad (\text{S1.4})$$

where the BdG Hamiltonian reads

$$H_\Delta = \begin{pmatrix} 0 & h_\Delta \\ h_\Delta^\dagger & 0 \end{pmatrix}, \quad h_\Delta = \begin{pmatrix} \Delta_s & 0 & \tilde{\Delta}_s & 0 \\ 0 & \Delta_s & 0 & \tilde{\Delta}_s \\ \tilde{\Delta}_s & 0 & \Delta_s & 0 \\ 0 & \tilde{\Delta}_s & 0 & \Delta_s \end{pmatrix}. \quad (\text{S1.5})$$

At low energy, the whole Nambu spinor containing 16 components in real space can be written as

$$\Psi(\mathbf{r}) = [\Psi_{1,\mathbf{q}}(\mathbf{r}), \Psi_{2,\mathbf{q}}(\mathbf{r}), \Psi_{3,\mathbf{q}}(\mathbf{r}), \Psi_{4,\mathbf{q}}(\mathbf{r}), \Psi_{1,\mathbf{q}}^*(\mathbf{r}), \Psi_{2,\mathbf{q}}^*(\mathbf{r}), \Psi_{3,\mathbf{q}}^*(\mathbf{r}), \Psi_{4,\mathbf{q}}^*(\mathbf{r})]^T. \quad (\text{S1.6})$$

where $|\mathbf{q}| \ll k_0, \beta$ and the basis functions for the Weyl nodes read

$$\Psi_{1,\mathbf{q}}(\mathbf{r}) = [\psi_{1,\uparrow}(\mathbf{r}), \psi_{1,\downarrow}(\mathbf{r})] = e^{i\beta x + ik_0 z} e^{i\mathbf{q} \cdot \mathbf{r}} \begin{bmatrix} c_{\uparrow}^{(B)} \\ c_{\downarrow}^{(A)} \end{bmatrix}, \quad (\text{S1.7})$$

$$\Psi_{2,\mathbf{q}}(\mathbf{r}) = [\psi_{2,\uparrow}(\mathbf{r}), \psi_{2,\downarrow}(\mathbf{r})] = e^{-i\beta x - ik_0 z} e^{i\mathbf{q} \cdot \mathbf{r}} \begin{bmatrix} c_{\uparrow}^{(A)} \\ c_{\downarrow}^{(B)} \end{bmatrix}, \quad (\text{S1.8})$$

$$\Psi_{3,\mathbf{q}}(\mathbf{r}) = [\psi_{3,\uparrow}(\mathbf{r}), \psi_{3,\downarrow}(\mathbf{r})] = e^{i\beta x - ik_0 z} e^{i\mathbf{q} \cdot \mathbf{r}} \begin{bmatrix} c_{\uparrow}^{(B)} \\ c_{\downarrow}^{(A)} \end{bmatrix}, \quad (\text{S1.9})$$

$$\Psi_{4,\mathbf{q}}(\mathbf{r}) = [\psi_{4,\uparrow}(\mathbf{r}), \psi_{4,\downarrow}(\mathbf{r})] = e^{-i\beta x + ik_0 z} e^{i\mathbf{q} \cdot \mathbf{r}} \begin{bmatrix} c_{\uparrow}^{(A)} \\ c_{\downarrow}^{(B)} \end{bmatrix}. \quad (\text{S1.10})$$

The projection of the pairing potential onto the Nambu spinor (S1.6) is calculated as

$$H_{ij}^S = \int d\mathbf{r} \psi_i^*(\mathbf{r}) H_S \psi_j(\mathbf{r}), \quad (\text{S1.11})$$

where ψ_i is the i -th component of the Nambu spinor (S1.6). For illustrations, $H_{1,10}^S$ and $H_{1,12}^S$ are given by

$$\begin{aligned} H_{1,10}^S &= \frac{1}{\Omega_0} \int d^3\mathbf{r} e^{-i\beta x - ik_0 z} e^{-i\mathbf{q} \cdot \mathbf{r}} (0, 0, 1, 0, 0, 0, 0, 0) H_\Delta (0, 0, 0, 0, 1, 0, 0, 0)^T e^{-i\beta x - ik_0 z} e^{i\mathbf{q} \cdot \mathbf{r}} \\ &= \frac{\tilde{\Delta}_s}{\Omega_0} \int d^3\mathbf{r} e^{-2i\beta x - 2ik_0 z} = 0, \end{aligned} \quad (\text{S1.12})$$

and

$$H_{1,12}^S = \frac{1}{\Omega_0} \int d^3\mathbf{r} e^{-i\beta x - ik_0 z} e^{-i\mathbf{q}\cdot\mathbf{r}} (0, 0, 1, 0, 0, 0, 0, 0) H_\Delta (0, 0, 0, 0, 0, 0, 1, 0)^T e^{i\beta x + ik_0 z} e^{i\mathbf{q}\cdot\mathbf{r}} = \Delta_s. \quad (\text{S1.13})$$

Here Ω_0 is the volume of the system. In calculating the element $H_{1,10}^S$, large length L_x or L_z of the system in the x or z direction or large Weyl-node separation k_0 or β are assumed such that $\beta L_x \gg 1$ or $k_0 L_z \gg 1$ and the integral vanishes. Along these lines, we obtain the 16×16 effective BdG Hamiltonian for the pairing:

$$H^S = \begin{pmatrix} 0 & 0 & h_S & 0 \\ 0 & 0 & 0 & h_S \\ h_S^\dagger & 0 & 0 & 0 \\ 0 & h_S^\dagger & 0 & 0 \end{pmatrix}, \quad h_S = \begin{pmatrix} 0 & 0 & 0 & \Delta_s \\ 0 & 0 & -\Delta_s & 0 \\ 0 & \Delta_s & 0 & 0 \\ -\Delta_s & 0 & 0 & 0 \end{pmatrix}. \quad (\text{S1.14})$$

We can see that the inter-orbital pairing vanishes as $\beta L_x \gg 1$ or $k_0 L_z \gg 1$. To physically understand the vanishing of the inter-orbital pairing, let us analyze the term $\psi_{\downarrow,\mathbf{k}}^{(A)} \psi_{\uparrow,-\mathbf{k}}^{(B)}$. According to the basis spinors of Weyl nodes (see the main text), $\psi_{\downarrow,\mathbf{k}}^{(A)}$ can corresponds to either $\psi_{1,\downarrow,\mathbf{k}}$ or $\psi_{3,\downarrow,\mathbf{k}}$, Weyl node 1 or 3. Then the $-\mathbf{k}$ in $\psi_{\uparrow,-\mathbf{k}}^{(B)}$ requires that $\psi_{\uparrow,-\mathbf{k}}^{(B)}$ must correspond to either Weyl node 2 or 4. This coupling, however, is not allowed since the B-orbital component of Weyl node 2 or 4 always carries \downarrow -spin. Similar analysis can be applied to the other three terms of the inter-orbital pairing. Therefore, at low energy the inter-orbital pairing $\tilde{\Delta}_s$ is suppressed and only the intra-orbital pairing Δ_s is important. From Eq. (S1.14), we can also observe that Δ_s couples Weyl nodes of the same chirality, i.e., Weyl node 1 to Weyl node 2 and Weyl node 3 to Weyl node 4. Thus, the whole effective BdG Hamiltonian decouples into four equivalent 4×4 blocks.

S2. TRANSPORT PROBABILITIES OF THE N-S JUNCTION

In this section, we apply the Blonder-Tinkham-Klapwijk theory [69] to calculate the transport probabilities.

Using one block of the BdG Hamiltonian, the Weyl N-S junction can be described by

$$h_{\text{BdG}} = \begin{pmatrix} -i\partial_z - \mu(z) & k_x - ik_y & \Delta_s(z) & 0 \\ k_x + ik_y & i\partial_z - \mu(z) & 0 & \Delta_s(z) \\ \Delta_s^*(z) & 0 & i\partial_z + \mu(z) & -k_x + ik_y \\ 0 & \Delta_s^*(z) & -k_x - ik_y & -i\partial_z + \mu(z) \end{pmatrix}, \quad (\text{S2.1})$$

in the basis $\Phi(\mathbf{r}) = [c_{1,\uparrow}(\mathbf{r}), c_{1,\downarrow}(\mathbf{r}), c_{2,\downarrow}(\mathbf{r}), -c_{2,\uparrow}(\mathbf{r})]^T$, where $\Delta_s(z) = \Delta e^{i\phi} \Theta(z)$ and $\mu(z) = \mu_N \Theta(-z) + \mu_S \Theta(z)$ with $\Delta > 0$ and $\Theta(z)$ the Heaviside step function.

On the WSM (N) side, the basis functions for a given excitation energy ε can be written as (we neglect the $e^{ik_x x + ik_y y}$ part for simplicity)

$$\varphi_{\vec{e}}(z) = (\cos \alpha_e, e^{i\theta_{\mathbf{k}}} \sin \alpha_e, 0, 0)^T e^{ik_e z}, \quad (\text{S2.2})$$

$$\varphi_{\overleftarrow{e}}(z) = (e^{-i\theta_{\mathbf{k}}} \sin \alpha_e, \cos \alpha_e, 0, 0)^T e^{-ik_e z}, \quad (\text{S2.3})$$

$$\varphi_{\vec{h}}(z) = (0, 0, -e^{-i\theta_{\mathbf{k}}} \sin \alpha_h, \cos \alpha_h)^T e^{ik_h z}, \quad (\text{S2.4})$$

$$\varphi_{\overleftarrow{h}}(z) = (0, 0, \cos \alpha_h, -e^{i\theta_{\mathbf{k}}} \sin \alpha_h)^T e^{-ik_h z}, \quad (\text{S2.5})$$

where $\theta_{\mathbf{k}} = \arctan(k_y/k_x)$, $\alpha_{e(h)} = \arctan(k_{\parallel}/k_{e(h)})/2$, and $k_{e(h)} = \text{sgn}(\varepsilon \pm \mu_N + k_{\parallel}) \sqrt{(\varepsilon \pm \mu_N)^2 - k_{\parallel}^2}$. On the superconducting (S) side, the basis functions are

$$\varphi_{\vec{e}q}(z) = (e^{i\beta} \cos \tilde{\alpha}_e, e^{i\beta} e^{i\theta_{\mathbf{k}}} \sin \tilde{\alpha}_e, e^{-i\phi} \cos \tilde{\alpha}_e, e^{-i\phi} e^{i\theta_{\mathbf{k}}} \sin \tilde{\alpha}_e)^T e^{ik_{eq} z}, \quad (\text{S2.6})$$

$$\varphi_{\overleftarrow{e}q}(z) = (e^{i\beta} e^{-i\theta_{\mathbf{k}}} \sin \tilde{\alpha}_e, e^{i\beta} \cos \tilde{\alpha}_e, e^{-i\phi} e^{-i\theta_{\mathbf{k}}} \sin \tilde{\alpha}_e, e^{-i\phi} \cos \tilde{\alpha}_e)^T e^{-ik_{eq} z}, \quad (\text{S2.7})$$

$$\varphi_{\vec{h}q}(z) = (e^{i\phi} e^{-i\theta_{\mathbf{k}}} \cos \tilde{\alpha}_h, e^{i\phi} \sin \tilde{\alpha}_h, e^{i\beta} e^{-i\theta_{\mathbf{k}}} \cos \tilde{\alpha}_h, e^{i\beta} \sin \tilde{\alpha}_h)^T e^{ik_{hq} z}, \quad (\text{S2.8})$$

$$\varphi_{\overleftarrow{h}q}(z) = (e^{i\phi} \sin \tilde{\alpha}_h, e^{i\phi} e^{i\theta_{\mathbf{k}}} \cos \tilde{\alpha}_h, e^{i\beta} \sin \tilde{\alpha}_h, e^{i\beta} e^{i\theta_{\mathbf{k}}} \cos \tilde{\alpha}_h)^T e^{-ik_{hq} z}, \quad (\text{S2.9})$$

where $\tilde{\alpha}_{e(h)} = \arctan(k_{\parallel}/k_{eq(hq)})/2$, and $k_{eq(hq)} = \text{sgn}\{\varepsilon \pm \text{sgn}(\mu_S \pm k_{\parallel})\sqrt{\Delta^2 + (\mu_S \pm k_{\parallel})^2}\} \sqrt{(\mu_S \pm \Omega)^2 - k_{\parallel}^2}$. For subgap energies $\varepsilon \leq \Delta$, $\beta = \arccos(\varepsilon/\Delta)$ and $\Omega = i\sqrt{\Delta^2 - \varepsilon^2}$ while, for supragap energies $\varepsilon > \Delta$, $\beta = -i\text{arccosh}(\varepsilon/\Delta)$ and $\Omega = \text{sgn}(\varepsilon)\sqrt{\varepsilon^2 - \Delta^2}$. Note that $\alpha_{e(h)}$ is always real while $\tilde{\alpha}_{e(h)}$ can be complex.

At an excitation energy $\varepsilon \geq 0$, the wave function, for the scattering state of an electron injected from the WSM and moving towards the interface, can be described by

$$\Psi(z) = \begin{cases} \varphi_{\vec{e}}(z) + b_0 \varphi_{\vec{e}}(z) + a_0 \varphi_{\vec{h}}(z), & z < 0 \\ c_0 \varphi_{\vec{e}q}(z) + d_0 \varphi_{\vec{h}q}(z), & z > 0 \end{cases} \quad (\text{S2.10})$$

where a_0 , b_0 , c_0 , and d_0 represent the coefficients of Andreev and normal reflections, transmissions to two right-moving quasi-particles, respectively. These coefficients are determined by the continuity of the wave functions at the N-S interface

$$\Psi(z = 0^+) = \Psi(z = 0^-). \quad (\text{S2.11})$$

With the basis functions and the coefficients, we can calculate the probabilities of Andreev and normal reflections, and transmissions which are defined by the Andreev and normal reflected, and transmitted current densities normalized by the incident current density, respectively. In general, the transport probabilities can be found, respectively, as

$$R_{eh}(\varepsilon, \mathbf{k}_{\parallel}) = \left| \frac{\sqrt{\cos(2\alpha_e) \cos(2\alpha_h)} \sin(\tilde{\alpha}_e - \tilde{\alpha}_h)}{e^{i\beta} \cos(\alpha_e + \tilde{\alpha}_e) \sin(\alpha_h + \tilde{\alpha}_h) - e^{-i\beta} \cos(\alpha_e + \tilde{\alpha}_h) \sin(\alpha_h + \tilde{\alpha}_e)} \right|^2, \quad (\text{S2.12})$$

$$R_{ee}(\varepsilon, \mathbf{k}_{\parallel}) = \left| \frac{e^{i\beta} \sin(\alpha_e - \tilde{\alpha}_e) \sin(\alpha_h + \tilde{\alpha}_h) - e^{-i\beta} \sin(\alpha_e - \tilde{\alpha}_h) \sin(\alpha_h + \tilde{\alpha}_e)}{e^{i\beta} \cos(\alpha_e + \tilde{\alpha}_e) \sin(\alpha_h + \tilde{\alpha}_h) - e^{-i\beta} \cos(\alpha_e + \tilde{\alpha}_h) \sin(\alpha_h + \tilde{\alpha}_e)} \right|^2, \quad (\text{S2.13})$$

$$T_{ee}(\varepsilon, \mathbf{k}_{\parallel}) = \left| e^{2i\beta} - 1 \right| \left| \frac{\sqrt{\cos(2\alpha_e)} (|\cos \tilde{\alpha}_e|^2 - |\sin \tilde{\alpha}_e|^2) \sin(\alpha_h + \tilde{\alpha}_h)}{e^{i\beta} \cos(\alpha_e + \tilde{\alpha}_e) \sin(\alpha_h + \tilde{\alpha}_h) - e^{-i\beta} \cos(\alpha_e + \tilde{\alpha}_h) \sin(\alpha_h + \tilde{\alpha}_e)} \right|^2, \quad (\text{S2.14})$$

$$T_{eh}(\varepsilon, \mathbf{k}_{\parallel}) = \left| e^{-2i\beta} - 1 \right| \left| \frac{\sqrt{\cos(2\alpha_e)} (|\cos \tilde{\alpha}_h|^2 - |\sin \tilde{\alpha}_h|^2) \sin(\alpha_h + \tilde{\alpha}_e)}{e^{i\beta} \cos(\alpha_e + \tilde{\alpha}_e) \sin(\alpha_h + \tilde{\alpha}_h) - e^{-i\beta} \cos(\alpha_e + \tilde{\alpha}_h) \sin(\alpha_h + \tilde{\alpha}_e)} \right|^2. \quad (\text{S2.15})$$

Eqs. (S2.12) and (S2.13) are the results [Eqs. (8) and (9)] given in the main text. In the Dirac system, on requiring the continuity of the wave function, the continuity of the current flux is also satisfied, as shown by $R_{ee} + R_{eh} + T_{ee} + T_{eh} = 1$. One can see clearly that for subgap energies $\varepsilon \leq \Delta$, β is real, thus there is no transmission probability, i.e., $T_{ee} = T_{eh} = 0$. In the following, we will analyze R_{eh} and R_{ee} , since they are the only functions required in the calculation of the differential conductance.

- For normal incidence with $\mathbf{k}_{\parallel} = 0$, $\alpha_e = \alpha_h = \tilde{\alpha}_e = 0$ and $\tilde{\alpha}_h = \pi/2$. Thus,

$$R_{eh}(\varepsilon, 0) = |e^{-2i\beta}|, \quad R_{ee}(\varepsilon, 0) = 0. \quad (\text{S2.16})$$

Andreev reflection dominates, i.e., $R_{eh} = 1$, for subgap energies whereas it decays to zero with increasing $\varepsilon > \Delta$.

- For $\mu_N, \mu_S \ll \Delta$ and $\mu_N < \varepsilon < \Delta$, $\alpha_h = \alpha_e$, $\tilde{\alpha}_h - \tilde{\alpha}_e = \pi/2$, $\cos(2\alpha_e) = \sqrt{\varepsilon^2 - k_{\parallel}^2}/\varepsilon$, $\sin(2\alpha_e) = k_{\parallel}/\varepsilon$, $\cos(2\tilde{\alpha}_e) = \sqrt{\Delta^2 - \varepsilon^2 + k_{\parallel}^2}/\sqrt{\Delta^2 - \varepsilon^2}$ and $\sin(2\tilde{\alpha}_e) = -ik_{\parallel}/\sqrt{\Delta^2 - \varepsilon^2}$. Thus,

$$R_{eh}(\varepsilon, \mathbf{k}_{\parallel}) = 1, \quad R_{ee}(\varepsilon, \mathbf{k}_{\parallel}) = 0. \quad (\text{S2.17})$$

This indicates that specular Andreev reflection dominates in the region $\mu_N < \varepsilon < \Delta$, leading to $g_{NS} = 2$.

- At $\varepsilon = \Delta$, $\beta = 0$ and $\tilde{\alpha}_h - \tilde{\alpha}_e = \pi/2$. Thus,

$$R_{eh}(\Delta, \mathbf{k}_{\parallel}) = \frac{\cos(2\alpha_e) \cos(2\alpha_h)}{\cos^2(\alpha_e - \alpha_h)}, \quad R_{ee}(\Delta, \mathbf{k}_{\parallel}) = \frac{\sin^2(\alpha_e + \alpha_h)}{\cos^2(\alpha_e - \alpha_h)}, \quad (\text{S2.18})$$

where the dependence on $\tilde{\alpha}_e$ and $\tilde{\alpha}_h$ cancels out. The reflection probabilities at excitation energy $\varepsilon = \Delta$ and hence the differential conductance at bias $eV = \Delta$ become independent of μ_S . If $\mu_N \ll \Delta$, then $\alpha_h = \alpha_e$ and

$$R_{eh}(\Delta, \mathbf{k}_{\parallel}) = 1 - |k_{\parallel}/\Delta|^2, \quad R_{ee}(\Delta, \mathbf{k}_{\parallel}) = |k_{\parallel}/\Delta|^2. \quad (\text{S2.19})$$

Plugging Eqs. (S2.19) in Eq. (11) in the main text gives rise to $g_{\text{NS}} = 1$. Therefore, for $\mu_N, \mu_S \ll \Delta$, g_{NS} shows a jump from 1 to 2 at $eV = \Delta$. For $\mu_S, \mu_N < \Delta$, the jump at $eV = \Delta$ still appears, but with a smaller discontinuous value.

- At $\varepsilon = \mu_N < \Delta$, Eqs. (S2.12) and (S2.13) simplify to

$$R_{eh}(\mu_N, \mathbf{k}_{\parallel}) = 0, \quad R_{ee}(\mu_N, \mathbf{k}_{\parallel}) = 1. \quad (\text{S2.20})$$

Andreev reflection is not allowed physically because there is no hole state on the N side. As a result, the differential conductance vanishes. The critical energy $\varepsilon = \mu_N$ separates two energy regions. In the region $\varepsilon < \mu_N$, Andreev retroreflection occurs while in the region $\varepsilon > \mu_N$, specular Andreev reflection occurs.

- At zero energy $\varepsilon = 0$, $\beta = \pi/2$, $\alpha_h = -\alpha_e$, $\sin \tilde{\alpha}_h = \cos^* \tilde{\alpha}_e$, and $\cos \tilde{\alpha}_h = \sin^* \tilde{\alpha}_e$. Thus,

$$R_{eh}(0, \mathbf{k}_{\parallel}) = \left| \frac{\cos(2\alpha_e)(|\sin \tilde{\alpha}_e|^2 - |\cos \tilde{\alpha}_e|^2)}{|\cos(\alpha_e + \tilde{\alpha}_e)|^2 + |\sin(\alpha_e - \tilde{\alpha}_e)|^2} \right|^2, \quad R_{ee}(0, \mathbf{k}_{\parallel}) = \left| \frac{2\sin(\alpha_e - \tilde{\alpha}_e)\cos(\alpha_e + \tilde{\alpha}_e)}{|\cos(\alpha_e + \tilde{\alpha}_e)|^2 + |\sin(\alpha_e - \tilde{\alpha}_e)|^2} \right|^2. \quad (\text{S2.21})$$

In the regime $|\mu_N| \ll \sqrt{\Delta^2 + \mu_S^2}$, since only the channels with real k_e and $k_{\parallel} < |\mu_w|$ are relevant, we have $k_{\parallel} \ll |\mu_N \pm \Omega|$ and $\tilde{\alpha}_e \approx 0$. Thus, R_{eh} and R_{ee} further simplify to

$$R_{eh}(0, \mathbf{k}_{\parallel}) = 1 - |k_{\parallel}/\mu_N|^2, \quad R_{ee}(0, \mathbf{k}_{\parallel}) = |k_{\parallel}/\mu_N|^2, \quad (\text{S2.22})$$

which become functions of a single parameter k_{\parallel}/μ_N and lead to the universal conductance e^2/h per unit channel.

S3. ANALOGY OF THE WEYL JUNCTION TO A 1D F-S JUNCTION

To see the role played by spin/orbital-momentum locking and s-wave pairing in the universal conductance e^2/h , it is instructive to consider a 1D Dirac F-S junctions. The 1D F-S junction with a ferromagnet on the negative side ($z < 0$) and a superconductor ($z > 0$) on the positive side can be described by

$$h_{\text{BdG}}^{(m)} = \begin{pmatrix} -i\partial_z - \mu(z) & m(z) & \Delta(z) & 0 \\ m(z) & i\partial_z - \mu(z) & 0 & \Delta(z) \\ \Delta(z) & 0 & i\partial_z + \mu(z) & -m(z) \\ 0 & \Delta(z) & -m(z) & -i\partial_z + \mu(z) \end{pmatrix}, \quad (\text{S3.1})$$

where $m(z) = m_0\Theta(-z)$, $\Delta(z) = \Delta\Theta(z)$ and $\mu(z) = \mu_F\Theta(-z) + \mu_S\Theta(z)$. Here the basis is $\Psi = (c_{1,\uparrow}, c_{1,\downarrow}, c_{2,\uparrow}^\dagger, -c_{2,\uparrow}^\dagger)^T$ with 1 and 2 denoting two valleys. Note that the magnetization $m(z)$ is valley dependent, i.e., it is opposite at the two valleys, and the pairing potential $\Delta(z)$ couples the same chirality (defined by the projection of the momentum onto the spin orientation). This is important to mimic the physics of the Weyl junction.

At zero excitation energy, the basis functions of the right-moving electron, left-moving electron and left-moving hole on the ferromagnetic side $z < 0$ are given by

$$\varphi_{m\vec{e}}(z) = (\cos \alpha_m, \sin \alpha_m, 0, 0)^T e^{ik_m z}, \quad (\text{S3.2})$$

$$\varphi_{m\leftarrow e}(z) = (\sin \alpha_m, \cos \alpha_m, 0, 0)^T e^{-ik_m z}, \quad (\text{S3.3})$$

$$\varphi_{m\leftarrow h}(z) = (0, 0, \cos \alpha_m, \sin \alpha_m)^T e^{ik_m z}, \quad (\text{S3.4})$$

respectively, where $\alpha_m = \arctan(m_0/k_m)/2$ and $k_m = \text{sgn}(\mu_F)\sqrt{\mu_F^2 - m_0^2}$. Note that these zero-energy states on the ferromagnetic side exist only when $m_0 < |\mu_F|$. Thus, in the following calculation, we focus on the case of $m_0 < |\mu_F|$. On the S side, the basis functions of the two “right-moving” particles are given by

$$\varphi_{m\vec{e}q}(z) = (i, 0, 1, 0)^T e^{i\tilde{k}_{eq}z}, \quad (\text{S3.5})$$

$$\varphi_{m\vec{h}q}(z) = (0, 1, 0, i)^T e^{-i\tilde{k}_{eq}z}, \quad (\text{S3.6})$$

where $\tilde{k}_{eq} = |\mu_S| + i\Delta$. Both $\varphi_{\vec{e}q}(z)$ and $\varphi_{\vec{h}q}(z)$ decay from the interface in the superconductor as $e^{-z/\xi}$ with $\xi = 1/\Delta$.

The matching of the wave function at the interface, $z = 0$, gives rise to the equation

$$\varphi_{m\vec{e}}(0) + b_0\varphi_{m\leftarrow{e}}(0) + a_0\varphi_{m\leftarrow{h}}(0) = c_0\varphi_{m\vec{e}q}(0) + d_0\varphi_{m\vec{h}q}(0), \quad (\text{S3.7})$$

where a_0, b_0, c_0 and d_0 , similar to the previous section, represent the coefficients of Andreev reflection, normal reflection and transmissions, respectively. The coefficients of Andreev and normal reflections are found as

$$a_0 = -i\sqrt{1 - |m_0/\mu_F|^2}, \quad b_0 = -m_0/\mu_F. \quad (\text{S3.8})$$

Then, the probabilities of Andreev and normal reflections are given by

$$R_{eh} = 1 - |m_0/\mu_F|^2, \quad R_{ee} = |m_0/\mu_F|^2, \quad (\text{S3.9})$$

respectively. Eq. (S3.9) indicates that in the absence of magnetization, $m_0 = 0$, the 1D junction exhibits perfect Andreev reflection, as expected by the conservation of chirality. A finite magnetization couples the right and left movers (i.e., different orbitals) and leads to finite normal reflection. The μ_S and Δ dependence disappear in the final results (S3.8) and (S3.9) because the space-dependent phases of the wave functions drop out in the continuity equation (S3.7). Most importantly, one can find that Eqs. (S3.9) resemble the form of Eqs. (S2.22) but with k_{\parallel} replaced by the magnetization m_0 . As a contrast, if the pairing potential couples opposite chirality (e.g., spin-triplet) or if the magnetization is valley independent, then following the same approach, one would find different results.

In the large-momentum mismatch regime $|\mu_N| \ll \sqrt{\Delta^2 + \mu_S^2}$ of the Weyl N-S junction, the parallel spin/orbital-momentum locking is significant on the N side but negligible on the S side, thus the system becomes equivalent to a bundle of 1D Dirac F-S junctions where the wave vector \mathbf{k}_{\parallel} acts as the valley-dependent parallel magnetization. In this way, one can see that the universal conductance e^2/h per unit channel is due to the interplay of the unique spin/orbital momentum locking and s-wave pairing that couples Weyl nodes of the same chirality.

S4. EFFECT OF A NON-MAGNETIC INTERFACE BARRIER

In the presence of an interface barrier, the junction can still be described by the BdG Hamiltonian (S2.1) but with

$$\Delta_s(z) = \Delta e^{i\phi}\Theta(z), \quad (\text{S4.1})$$

$$\mu(z) = \mu_N\Theta(-z) + \mu_S\Theta(z) - V_0\Theta(z+d)\Theta(-z). \quad (\text{S4.2})$$

Here the length d and potential V_0 of the barrier are assumed to satisfy

$$d \rightarrow 0 \text{ and } V_0 \rightarrow \infty, \quad (\text{S4.3})$$

such that the dimensionless barrier strength $\chi = V_0d$ remain finite [74].

On the N and S sides, the basis functions are still given by Eqs. (S2.2-S2.5) and (S2.6-S2.9), respectively. On the barrier, $0 < z < d$, the basis functions can be written as

$$\varphi'_{\vec{e}}(z) = (1, 0, 0, 0)^T e^{-iV_0z}, \quad (\text{S4.4})$$

$$\varphi'_{\leftarrow{e}}(z) = (0, 1, 0, 0)^T e^{iV_0z}, \quad (\text{S4.5})$$

$$\varphi'_{\vec{h}}(z) = (0, 0, 0, 1)^T e^{iV_0z}, \quad (\text{S4.6})$$

$$\varphi'_{\leftarrow{h}}(z) = (0, 0, 1, 0)^T e^{-iV_0z}. \quad (\text{S4.7})$$

Note that these expressions are valid only for the limit (S4.3).

For an excitation energy $\varepsilon \geq 0$, the wave function, for the scattering state for an electron injected in the WSM and moving right to the barrier, is described by

$$\Psi(z) = \begin{cases} \varphi_{\vec{e}}(z) + a_0\varphi_{\leftarrow{e}}(z) + b_0\varphi_{\leftarrow{h}}(z), & z < -d \\ A\varphi'_{\vec{e}}(z) + B\varphi'_{\leftarrow{e}}(z) + C\varphi'_{\leftarrow{h}}(z) + D\varphi'_{\vec{h}}(z), & -d < z < 0 \\ c_0\varphi_{\vec{e}q}(z) + d_0\varphi_{\vec{h}q}(z), & z > 0 \end{cases} \quad (\text{S4.8})$$

The coefficients, $a_0, b_0, c_0, d_0, A, B, C$, and D are found by matching the wave function at the two interfaces $z = -d$ and $z = 0$. Then, the Andreev and normal reflection probabilities are obtained, respectively, as

$$R_{eh}(\varepsilon, \mathbf{k}_{\parallel}) = |\cos(2\alpha_e) \cos(2\alpha_h)| |\sin(\tilde{\alpha}_e - \tilde{\alpha}_h) / \mathcal{Z}'|^2, \quad (\text{S4.9})$$

$$R_{ee}(\varepsilon, \mathbf{k}_{\parallel}) = |\mathcal{Y}' / \mathcal{Z}'|^2, \quad (\text{S4.10})$$

where

$$\begin{aligned} \mathcal{Z}' = & e^{i\beta} (e^{-i\chi} \sin \alpha_e \sin \tilde{\alpha}_e - e^{i\chi} \cos \alpha_e \cos \tilde{\alpha}_e) (e^{i\chi} \sin \alpha_h \cos \tilde{\alpha}_h + e^{-i\chi} \cos \alpha_h \sin \tilde{\alpha}_h) \\ & - e^{-i\beta} (e^{-i\chi} \sin \alpha_e \sin \tilde{\alpha}_h - e^{i\chi} \cos \alpha_e \cos \tilde{\alpha}_h) (e^{i\chi} \sin \alpha_h \cos \tilde{\alpha}_e + e^{-i\chi} \cos \alpha_h \sin \tilde{\alpha}_e), \end{aligned} \quad (\text{S4.11})$$

$$\begin{aligned} \mathcal{Y}' = & e^{i\beta} (e^{-i\chi} \cos \alpha_e \sin \tilde{\alpha}_e - e^{i\chi} \sin \alpha_e \cos \tilde{\alpha}_e) (e^{i\chi} \sin \alpha_h \cos \tilde{\alpha}_h + e^{-i\chi} \cos \alpha_h \sin \tilde{\alpha}_h) \\ & - e^{-i\beta} (e^{-i\chi} \cos \alpha_e \sin \tilde{\alpha}_h - e^{i\chi} \sin \alpha_e \cos \tilde{\alpha}_h) (e^{i\chi} \sin \alpha_h \cos \tilde{\alpha}_e + e^{-i\chi} \cos \alpha_h \sin \tilde{\alpha}_e). \end{aligned} \quad (\text{S4.12})$$

We can see that R_{eh} and R_{ee} are periodic functions of χ with a period π . Thus, the differential conductance is also a periodic function of χ . Under the condition $\chi = N\pi$, $N = 0, \pm 1, \pm 2, \dots$, the expressions (S4.9) and (S4.10) reproduce the results Eqs. (S2.12) and (S2.13) in the absence of the barrier.

At zero excitation energy $\varepsilon = 0$, $\beta = \pi/2$, $\alpha_h = -\alpha_e$, $\sin \tilde{\alpha}_h = \cos^* \tilde{\alpha}_e$ and $\cos \tilde{\alpha}_h = \sin^* \tilde{\alpha}_e$. Thus,

$$R_{eh}(0, \mathbf{k}_{\parallel}) = \left| \frac{\cos(2\alpha_e) (|\sin \tilde{\alpha}_e|^2 - |\cos \tilde{\alpha}_e|^2)}{|e^{-i\chi} \sin \alpha_e \sin \tilde{\alpha}_e - e^{i\chi} \cos \alpha_e \cos \tilde{\alpha}_e|^2 + |e^{i\chi} \sin \alpha_e \cos \tilde{\alpha}_e - e^{-i\chi} \cos \alpha_e \sin \tilde{\alpha}_e|^2} \right|^2, \quad (\text{S4.13})$$

$$R_{ee}(0, \mathbf{k}_{\parallel}) = \left| \frac{(e^{i\chi} \sin \alpha_e \cos \tilde{\alpha}_e - e^{-i\chi} \cos \alpha_e \sin \tilde{\alpha}_e) (e^{i\chi} \cos \alpha_e \cos \tilde{\alpha}_e - e^{-i\chi} \sin \alpha_e \sin \tilde{\alpha}_e)}{|e^{-i\chi} \sin \alpha_e \sin \tilde{\alpha}_e - e^{i\chi} \cos \alpha_e \cos \tilde{\alpha}_e|^2 + |e^{i\chi} \sin \alpha_e \cos \tilde{\alpha}_e - e^{-i\chi} \cos \alpha_e \sin \tilde{\alpha}_e|^2} \right|^2. \quad (\text{S4.14})$$

We now focus on the regime $|\mu_N| \ll \sqrt{\Delta^2 + \mu_S^2}$. Since we are considering the channels with real k_e and $k_{\parallel} < |\mu_w|$, we have $k_{\parallel} \ll |\mu_N \pm \Omega|$ and $\tilde{\alpha}_e \approx 0$. R_{eh} and R_{ee} further simplify to

$$R_{eh}(0, \mathbf{k}_{\parallel}) = 1 - |k_{\parallel} / \mu_N|^2, \quad R_{ee}(0, \mathbf{k}_{\parallel}) = |k_{\parallel} / \mu_N|^2, \quad (\text{S4.15})$$

which are the same results as those in the absence of the barrier. The barrier becomes effectively transparent in the regime $|\mu_N| \ll \sqrt{\Delta^2 + \mu_S^2}$. As a result, the contributions of Andreev and normal reflections cancel perfectly and the zero-bias differential conductance can still acquire the universal value e^2/h per unit channel.